Analysis of Screen Channel LAD Bubble Point Tests in Liquid Methane at Elevated Temperature

Jason Hartwig[1]
ASRC Aerospace, Cleveland, OH, 44135, USA

John McQuillen[2]
NASA Glenn Research Center at Lewis Field, Cleveland, OH, 44135, USA

This paper examines the effect of varying the liquid temperature and pressure on the bubble point pressure for screen channel Liquid Acquisition Devices in cryogenic liquid methane using gaseous helium across a wide range of elevated pressures and temperatures. Testing of a 325 x 2300 Dutch Twill screen sample was conducted in the Cryogenic Components Lab 7 facility at the NASA Glenn Research Center in Cleveland, Ohio. Test conditions ranged from 105 to 160K and 0.0965 – 1.78 MPa. Bubble point is shown to be a strong function of the liquid temperature and a weak function of the amount of subcooling at the LAD screen. The model predicts well for saturated liquid but under predicts the subcooled data.

Nomenclature

D_p	=	pore diameter [μm]
T_c	=	Critical temperature [K]
ΔP_{BP}	=	Bubble point pressure [in H_2O]
$\Delta P_{dynamic}$	=	Pressure loss for mass accumulation along channel length
$\Delta P_{friction}$	=	Friction pressure loss for flow along channel
ΔP_{FTS}	=	Pressure loss for flow through screen
$\Delta P_{hydrostatic}$	=	Hydrostatic pressure
ΔP_{Other}	=	Other sources of pressure fluctuations and differences
σ	=	Surface tension [N/m]
θ_c	=	Contact angle

I. Introduction

GRAVITY affects the positioning of the liquid and vapor phases within a propellant tank. In a standard 1-g environment, the heavier fluid (liquid) tends toward the bottom and the lighter fluid (vapor) tends toward the top of the tank. In a reduced gravity environment however, surface tension becomes the controlling mechanism for this phase separation. For wetting systems, the liquid tends to wrap the walls, leaving an interior void consisting of a pressurant gas and vapor, resulting in little or no vapor contact with the walls of the tank.

When feeding propellant from the storage tank to a spacecraft engine in reduced gravity, it is necessary to transfer only the single phase liquid to ensure efficient thermal conditioning and the safe and stable operation of the engine after ignition. In Earth's 1-g field, or under a significant thruster firing in low gravity, propellant transfer is straightforward. Single phase liquid can be

[1] Research Aerospace Engineer, Propellants and Propulsion Branch, 21000 Brookpark Road, MS 500-1, Cleveland, OH 44135, and AIAA Member.
[2] Senior Aerospace Engineer, Fluid Physics and Transport Branch, 21000 Brookpark Road, MS 77-5, Cleveland, OH 44135, Non-Member.

obtained through the use of a collection sump and an anti-vortex baffle over the tank outlet. Fluid is transferred by simply opening a valve at the bottom of the tank. In low gravity, however, where fluid may not sufficiently envelop the tank outlet, supplying single phase liquid flow becomes a challenge. Depending on the vehicle, mission requirements, and gravitational environment, several different propellant management devices (PMD) may be required for liquid delivery.

One PMD used to collect single phase liquid from the propellant tank is the screen channel Liquid Acquisition Device (LAD). These LADs rely on capillary flow and surface tension forces to wick fluid into a channel, and to maintain a barrier to gas ingestion as liquid is expelled from a tank. Screen channel LADs tend to follow the contours of the tank, with various channels or "gallery arms", which extend along the entire tank to ensure total communication at all times between liquid propellant and tank outlet during outflow. Total communication screen style LADs have demonstrated flight heritage in storable propellant propulsion systems, such as the Space Shuttle Reaction Control System/Orbital Maneuvering System (Fester et. al 1975 and Peterson and Uney 1978), but no flight heritage in liquid oxygen (LOX) or liquid methane (LCH_4).

Screen channel LADs are generally characterized by the screen weave, which refers to the number of wires per inch in each direction and the specific wire pattern. For the 325x2300 Dutch Twill screen, each weft wire passes over two warp wires before going under the next warp wire. A fine mesh screen is desirable to ensure adequate wicking of liquid into the screen pores and to act as a barrier to vapor ingestion. However, fine mesh screens tend to generate larger viscous pressure losses through the screen during outflow. Thus far, no single screen style exists to optimize the PMD subsystem for all propellants or missions.

II. Background

For traditional cryogenic propellant systems, liquid oxygen/liquid hydrogen (LOX/LH_2) has been the preferred choice, since it has the highest specific impulse (ISP) of all propellant combinations. Recently, there has been a growing desire to develop technology to enable pressure-fed cryogenic propellant engines to take advantage of potential higher engine performance at higher operating pressures. As an alternative to storable propulsion systems (i.e. propellants that exist as a liquid at room temperature), trade studies were conducted to evaluate the feasibility of utilizing LOX/LCH_4 propellants for the Altair ascent stage propulsion system (Dickens 2010). This option considered the use of high pressure propellant tanks and a natural pressure gradient between tank and engine to feed the ascent main engine (AME).

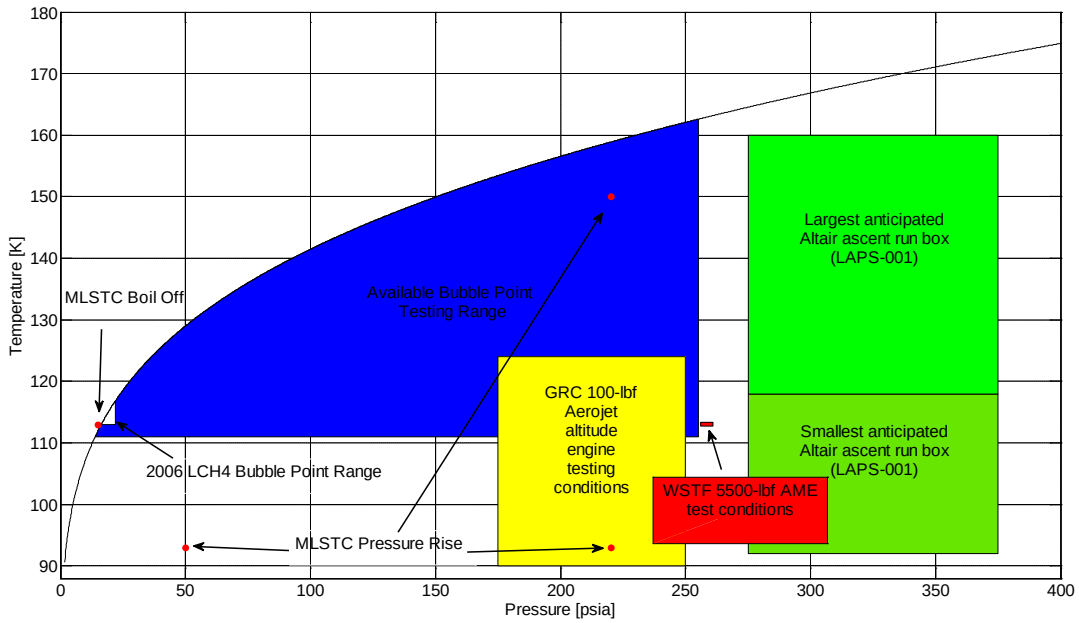

Figure 1 – Summary of the Primary Liquid Methane Analytical and Experimental Test Conditions under NASA's LOX/LCH_4 Technology Development Program

Figure 1 provides a summary of recent analysis and experiments conducted at NASA Glenn Research Center (GRC) and at White Sands Test Facilities (WSTF). Shown here are the initially anticipated Altair engine start box conditions from the Lunar Ascent Propulsion Systems (LAPS) studies (Dickens 2010), along with recently concluded LOX/LCH_4 altitude combustion engine testing conditions of a small scale 100-lbf (Marshall and Kleinhenz 2010) and large 5500-lbf AME (Stiegemeier et. al 2010). Also plotted are the propellant tank conditions from the Methane Lunar Surface Thermal Control (MLSTC) boil off and pressure rise tests (Plachta et. al 2012), previous low pressure methane bubble points from Jurns et. al (2007), and the saturation curve for methane.

The blue shaded region represents thermodynamic conditions at the LAD screen over which the current bubble point tests were conducted. The goal was to collect bubble breakthrough values over as wide a range as possible to give future mission designers direct bubble point data to characterize the LAD subsystem at any elevated temperature or pressure within the propellant tank. Instead of extrapolating screen channel LAD performance at these elevated conditions, it was determined that bubble point measurements needed to be conducted near these operating conditions, since there was discrepancy in surface tension data for cryogens from different published sources (e.g. Roder and Weber 1972). Given that the LAD performance in high pressure propellant tanks is likely affected by the pressurization method, bubble point data was collected over the widest possible range of thermal conditions inside a LCH4 propellant tank, consistent with the limitations of the test hardware as shown in Figure 1.

III. The Bubble Point

When vapor or pressurant penetrates into the channel, the LAD is said to have "broken down". This breakdown point or bubble point is defined as the differential pressure across a screen pore that overcomes the surface tension of the liquid at that pore. Parameters that affect the bubble point include the geometry and size of the pore, the contact angle between liquid and screen, and the surface tension of the liquid propellant, which is a function of temperature. Assuming that the pore geometry is a circular capillary tube, the bubble point may be expressed as:

$$\Delta P_{BP} = \frac{4\sigma \cos\theta}{D_P} \tag{1}$$

where σ is the surface tension of the fluid [N/m], θ_c is the contact angle formed between the liquid and the solid surface of the screen and D_P is the average pore diameter [m]. For cryogenic liquids and standard hydrophilic tank surfaces, $\theta_c \approx 0$. Previous studies have attempted to characterize pore diameters based on the wire geometry within the screen unsuccessfully (Jurns and McQuillen 2008). Therefore, the standard practice for estimating the pore diameter is to measure the bubble point using a reference fluid, such as isopropyl alcohol (IPA), and use similitude to determine D_P:

$$D_P = \frac{4\sigma_{IPA}}{\Delta P_{BP,IPA}} \tag{2}$$

During flow, the total pressure loss between the tank and the LAD channel outlet must be less than the bubble point pressure to prevent vapor ingestion into the channel. For a total communication gallery arm inside a propellant tank, the total pressure drop may be summed accordingly:

$$\Delta P_{Total} = \Delta P_{hydrostatic} + \Delta P_{FTS} + \Delta P_{friction} + \Delta P_{dynamic} + \Delta P_{other} \tag{3}$$

where $\Delta P_{hydrostatic}$ is the hydrostatic pressure on the LAD screen at the tank liquid vapor interface, ΔP_{FTS} is the pressure drop for flow through the screen, $\Delta P_{friction}$ is the frictional loss for flow along the LAD channel, $\Delta P_{dynamic}$ is the dynamic pressure drop due to the additional fluid entering the channel, and ΔP_{other} is the pressure loss contribution due to vibrations, propellant sloshing, and/or transients (Van Dyke 1998). Therefore, for the system conditions, cryogen and screen style, the bubble point is the upper limit on the total allowable pressure loss between the tank and the LAD channel outlet and serves as a primary performance parameter for screen channel LADs.

IV. Previously Reported Bubble Points

Historically, screens and screen channel LADs are well characterized for storable propellants and for cryogens at or near the saturated state at the low pressures typical of pump-fed engines. Previous experimental test programs conducted at GRC and Marshall Space Flight Center (MSFC) have characterized LADs for a variety of screen styles and cryogenic fluids. Figure 2 summarizes previously reported bubble point measurements for the 325x2300 Dutch

Twill screen sample for cryogenic LH_2, liquid nitrogen (LN_2), LOX, and LCH_4 at saturation pressures near standard conditions using gaseous helium (GHe) as the pressurant gas, as well as storable fluids such as IPA and Freon-112 as reported by Paynter (1973), Burge and Blackmon (1973), Cady (1973), Cady (1975), Cady (1977), Chato and Kudlac (2002), Kudlac and Jurns (2005), and Jurns et. al (2007). Also plotted in Figure 3 is the normal boiling point (NBP) prediction curve from Equation (1). With the exception of recently concluded high pressure LOX LADs and bubble points tests, the majority of the aforementioned tests were conducted under low pressure conditions where the liquid cryogen was close to the saturated state (Hartwig and McQuillen 2011). As shown, reasonable agreement exists between previous measurements and the bubble point prediction based on simple surface tension theory. The spread in the IPA data could be attributable to small variations from screen sample to sample.

Previous bubble point tests conducted in highly subcooled liquid (i.e. liquid that is maintained at a temperature lower than the saturation temperature based on the pressure at the screen) show that Equation (1) only holds for a normally saturated fluid (Hartwig and McQuillen 2011). Previous efforts to modify the bubble point equation for subcooled liquid were attempted by taking into account the fluid viscosity and density using a relationship developed by Bretherton (1961) for the slow motion of an elongated bubble through a capillary tube. While the analysis correlated well for subcooled liquid methane, Jurns and McQuillen (2008) found that this correction term did not hold when applied to results for subcooled liquid oxygen over the same small deviation from a saturated state. While there are reported values for LH_2, LN_2, and LOX from independent sources, the only known previously reported bubble points in LCH_4 are reported by Jurns et. al (2007).

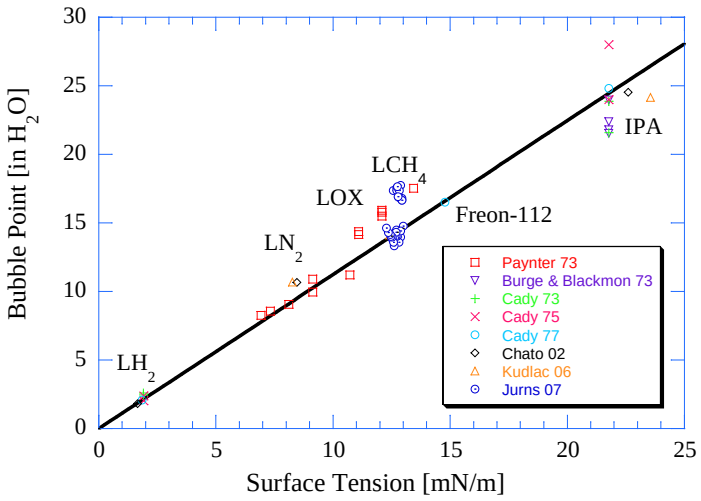

Figure 2: Previously Reported Bubble Point Values for the 325x2300 Dutch Twill Screen with Helium Pressurant

V. Description of Test Hardware

Testing was conducted in the Cryogenic Components Lab 7 (CCL-7) facility at GRC in Cleveland, Ohio. A single 325 x 2300 Dutch Twill screen sample was tested. The diameter of the warp and weft wires is 38.1 μm and 25.4 μm, respectively and the approximate thickness of the screen sample is 89 μm. In conjunction with Equation (2), bubble point tests in IPA were used to determine an effective pore diameter of 14.3 μm. The LAD screen sample was mounted onto a 2.38 cm tall, 5.08 cm (2") outer diameter (OD) cup. The liquid/vapor interface was formed within the screen pores by pressurizing the cup from below with vapor or gas.

The LAD screen and cup assembly was mounted inside of a 3.55 MPa (500 psig) rated, 15 cm (6") OD, 33.65 cm (13.25") high, optically accessible cryogenic fluid management (CFM) test tank. The CFM test tank was designed to contain high pressure LCH_4 above the test screen. The test tank was mounted inside a 56 cm (22'') OD, 107 cm (42'') tall, 0.229 m^3 (8.1 ft^3) receiver dewar (RD) as shown in Figure 3. The RD minimized parasitic heat leak into the test tank as there was no active external control of the temperature of the test tank. The vacuum jacket of the dewar was pumped down to full vacuum prior to every test, and CCL-7 air ejectors were used to decrease the pressure inside the RD to 0.10 kPa. Despite these measures, the pressure and temperature of the liquid would gradually increase, but multiple chill down cycles of the hardware prior to testing were utilized to establish the necessary test conditions. All critical pressure control and regulation was remotely controlled for reasons of safety. The RD lid had ten ports for the RD vacuum, test tank fill and drain, vent, the subcooling ejector, pressurization gas, three optical ports (camera and light source x2), and SD wires (x2), as shown in Figure 3. The CFM test tank was also equipped with several ports on top and below for liquid fill and drain, pressurization, back pressure control, instrumentation, and relief also shown in Figure 4.

Liquid methane was filled off site in portable 450 L dewars and was connected to the flow system through a flexible vacuum jacketed (VJ) line. To pressurize beneath the LAD screen, GHe was available from a portable tuber trailer and regulated to a delivery pressure between 0 – 250 psia. Gas pressure and flow rate were controlled by a set of two low flow control valves located directly upstream of the CFM test tank.

Pressure of the liquid inside the CFM test tank was controlled using a back pressure control valve or through the use of a mini-ejector. Pressure would also naturally rise due to heat leak into the test tank and was controlled by venting the tank to atmosphere. The ejectors were used to obtain sub-atmospheric pressure within the test tank. The liquid temperature inside the test tank was determined by the initial temperature of the liquid inside the portable LCH_4 dewar; however, the liquid could be conditioned to the saturation temperature via pressure control to between 0.101 to 1.82 MPa (14.7 to 265 psia). Thus, "cold" liquid was achieved by venting the dewar down to atmospheric pressure while "warm" liquid was achieved by allowing the dewar to warm over a period of days.

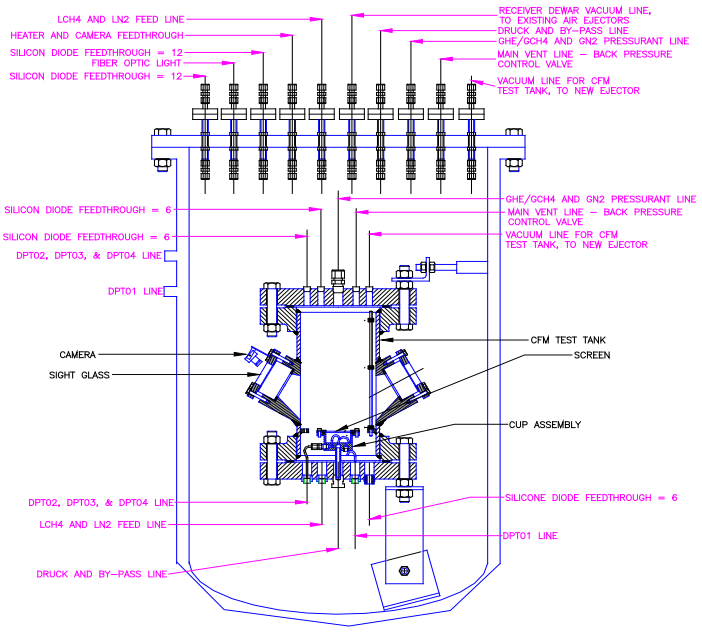

Figure 3: Dewar, CFM Test Tank, and LAD Screen/Cup Assembly

Temperature instrumentation is outlined in Figure 4, where numbers correspond to the diode locations. SD1 was mounted directly to the LAD screen on the liquid side of the interface while SD2 was attached to the gas side of the screen within the cup assembly. Both diodes were directly mounted to the LAD screen. SD3 measured the temperature of incoming pressurization gas. SD4 – 17 were spaced 0.5'' apart on a vertical rake within the liquid of the test tank and were used to measure both temperature and height of the bulk liquid. Using more diodes reduced uncertainty in the bubble point values by a factor of nearly 2 from previous measurements conducted in LOX.

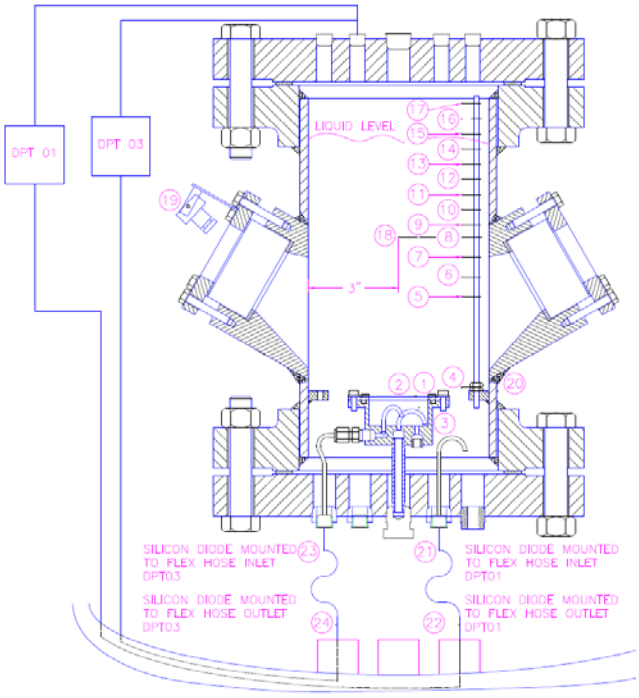

Figure 4: Location of Temperature Measurements inside CFM Test Tank

The pressure in the ullage space of the CFM test tank was measured using a 0-500 psia pressure transducer and three differential pressure transducers (DPT) were used to deduce the differential pressure across the LAD screen sample and liquid head pressure on top of the screen. DPT01 (0 – 5 psid) measured the pressure of the bottom of CFM test tank with respect to the ullage while DPT02 and DPT03 (0 – 30'' H_2O) provided redundant measurement of the pressure inside the LAD screen/cup assembly with respect to the ullage pressure.

The test tank was equipped with three thick quartz windows to allow imaging using a charge coupled device (CCD) camera and illumination from two light sources as shown in Figure 4. Real time images were time stamped with a resolution of 0.1 s, recorded, and monitored inside the test control room. Data channels were recorded at 4 Hz

using the data acquisition system and were synchronized with video data. All silicon diodes measured temperature to within +/- 0.5 K. The ullage pressure was within +/- 0.667 psia of the measured value. It is worth noting that there was less than 0.05 kPa (0.2 in H_2O) difference between DPT02 and DPT03 in all measured values. Liquid level measurements were accurate to within 6.35 mm (0.25 in) using the SDs. The DPT across the LAD screen sample measured pressure to within +/- 0.0104 kPa (0.042 in H_2O), which was less than 1% of the lowest measured bubble point. However, due to time synchronization errors, interpolation between time steps, and uncertainty in liquid level, the total uncertainty in reported bubble point values is estimated to be +/- 0.034 kPa (0.138 in H_2O), which was no higher than 3.1% at the warmest liquid temperature.

VI. Experimental Methodology

The methodology for conducting a bubble point test was as follows: Prior to filling the test tank, the RD was evacuated to minimize heat leak into the CFM test tank, and all flow lines and test hardware were purged with GHe. The cup was pressurized using GHe to prevent flooding of the cup during liquid transfer. The hardware was then initially pre-chilled several times using LN_2 to condition the system to the desired initial temperature and to limit the test hardware's rate of warming during testing. Liquid methane was then transferred into the test tank with an open vent value. After the tank was full, the vent valve was closed and the system was pressurized to the desired state. Prior to data collection, the LAD screen/cup assembly was purged with high pressure GHe to prevent flooding of the cup and instrumentation lines.

For each bubble point measurement, the screen was sealed by gradually decreasing the GHe flow underneath the screen until bubbling through the screen had stopped, resulting in liquid cryogen above the screen and gas maintained below the screen. Using the low flow control valves, the pressure underneath the screen was increased relative to the ullage pressure. The bubble point was taken as the moment that visible gas or vapor bubbles penetrated the screen mesh. Bubble penetration through the screen was detected visually and by the spike in the DPT03 signal, the time was noted and used to extract the exact bubble point pressure from the data file.

Bubble points were measured at similar tank pressures and/or temperatures for repeatability and consistency, and to reduce time synchronization error in the video file. In order to eliminate the possibility that bubble breakthrough was due to screen manufacturing variations or defects, measurements were repeated to verify that bubble breakthrough would occur at different locations on the screen.

Once testing was complete, any residual vapor was directly vented to atmosphere. Residual vapors trapped within the tank and flow lines were purged with GHe. The pressure in the RD was brought back to ambient conditions. Videos of the LAD screen were then transferred to an external hard drive.

With the exception of LOX bubble point tests by Hartwig and McQuillen (2011), bubble point tests for screen channel LADs have only been examined for saturated liquid conditions near the atmospheric boiling point. The high pressure test tank allowed examination of both subcooled and saturated liquid states at the LAD screen over a wide range of temperatures. Subcooled states were achievable by pressurizing the ullage space in the test tank or through the use of the mini ejector system. Bubble points were also obtained close to the saturation curve by allowing the hardware to warm over a period of several days, and immediately filling with cold liquid, thus maintaining the propellant in a boiling state as pressure increased over time. Thus it was possible to independently examine the temperature and pressure dependence of the bubble point over the whole blue shaded region from Figure 1. Tests were conducted between pressures of 0.069 MPa (10 psia) and 1.725 MPa (250 psia) and a temperature range of 105 – 160K.

All experimental bubble point values were reported by correcting the DPT03 reading for head pressure:

$$\Delta P_{BP}\left(T,P\right)\Big|_{\exp} = DPT03 - \rho_{LCH4} g LL \tag{4}$$

where g is the gravitational acceleration and LL is the liquid level in the CFM test tank as determined by the vertical silicon diode rake. Bubble points were reported using either the liquid screen side temperature or the bulk liquid temperature and using the pressure at the LAD screen.

Data reduction included determining the liquid level in the CFM test tank from plots of SD voltage vs. time and included interpolation to determine the liquid level between the sensing diodes. Exact bubble breakthrough times were determined from the videos. The pressure, temperature and flow rate sensor data were extracted from the corresponding time in the data file. Thermodynamic properties of interest, such as surface tension, density, and saturation temperature, were calculated using National Institute of Standards and Technology's (NIST) Reference Fluid Thermodynamic and Transport Properties Database: REFPROP. Parameters such as heat and mass transport at the screen were calculated during post processing.

VII. Results and Discussion

From December 2010 to January 2011, numerous bubble point tests were conducted over the range of conditions in the blue shaded region in Figure 1. Figure 9 plots the thermodynamic state of the liquid at the LAD screen during bubble breakthrough in terms of the pressure and temperature of the bulk liquid. As shown, bubble breakthrough across the LAD screen was achieved across the entire range of conditions for the proposed high pressure liquid methane propellant tank for GHe. There was little disparity between reporting the breakthrough point using either the screen or bulk liquid temperature for helium pressurization, which implies that the liquid at the screen and the bulk liquid were coupled before and during screen breakdown.

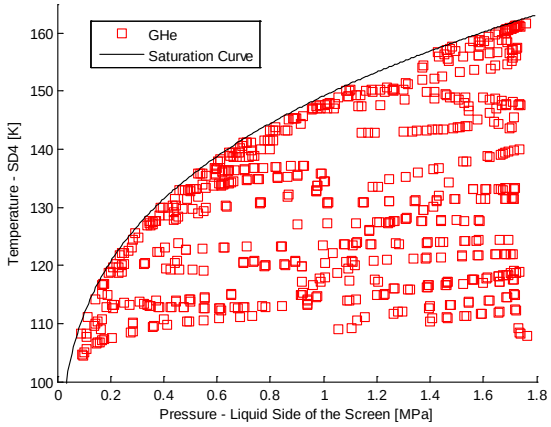

Figure 5: Thermodynamic Conditions at Bubble Breakthrough as a Function of the Pressure at the LAD Screen Temperature of the Bulk Liquid (SD4)

Figures 6a and b plot the experimentally obtained bubble point pressure as a function of the liquid screen side temperature and bulk liquid temperature, respectively, along with the prediction curve based on Equation 1 for zero contact angle. This comparison was based on observations by Hartwig and McQuillen (2011) for bubble breakthrough tests in LOX using both GHe and gaseous oxygen as a pressurant where there were noticeable differences in the plots. The predicted value of bubble point is calculated from surface tension based on the saturation temperature based on the pressure at the screen. The bubble point pressure decreases with increasing liquid temperature, due to decreasing surface tension of the liquid. The model qualitatively tracks this trend but under predicts the data by as much as 30%, especially at colder liquid temperatures. In light of this under prediction, Equation 1 may be used as a lower bound to predict screen channel LAD performance for a flight system, since the actual breakdown pressure is higher for all temperatures tested here. The bubble point represents the maximum allowable pressure drop before vapor is ingested into the channel and in the transfer line to the engine. Therefore results here imply that using GHe to pressurize and subcool the LCH_4 during expulsion results in higher margin in the total allowable pressure loss for the LAD system. Unlike the LOX data, a comparison of Figures 6a and 6b indicates that the correlation between the experimental data and model when using the liquid screen side temperature is no better than using the bulk liquid temperature. Nonetheless, for consistency with Hartwig and McQuillen (2011), it is proposed to correlate the bubble point with surface tension based on the liquid screen side temperature based on the partial pressure of LCH_4 at the screen.

The bulk of the scatter in the data in Figures 6a and b is attributed to the fact that bubble points at single temperatures were collected across a range of different pressures. Note that there is more variation in bubble point at

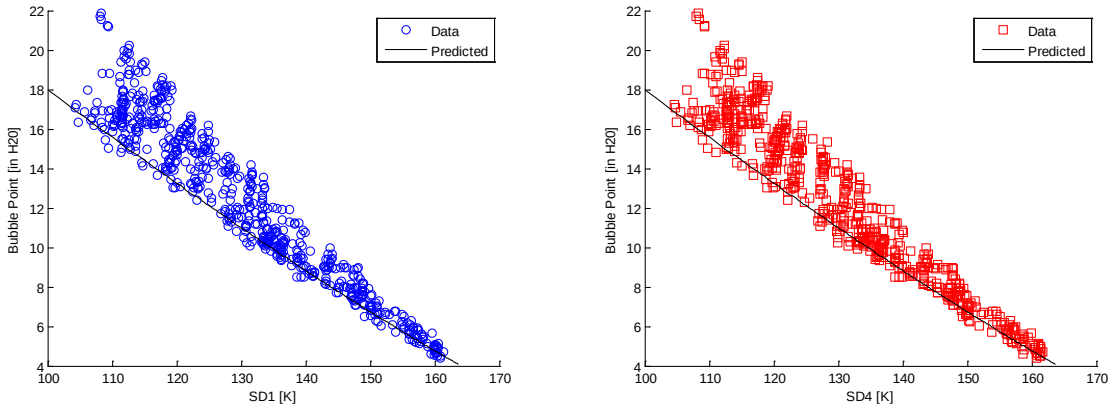

Figure 6: Bubble Point Pressure Reported as a Function of a) Temperature of the Liquid Side of the Screen (SD1) and b) Temperature of the Bulk Liquid (SD4) for the 325x2300 Sceren

colder liquid temperatures, which were achievable under a broad range of pressures, while there is less variation at warmer temperatures, which were only achievable at higher pressures within the facility limits. It should be noted that the apparent convergence of the bubble point data at elevated temperature is only a consequence of these system limitations.

Surface tension is generally known to be a function of temperature only, and of the form proposed by Ferguson and Kennedy (1936):

$$\sigma = \sigma_c (1 - \frac{T}{T_C})^K \tag{5}$$

Incorporating the temperature dependence of Equation 5 into Equation 1 indicates that the bubble point pressure has no pressure dependence. However, during transfer of liquid from the propellant tank through the LAD to the transfer line, the liquid temperature and pressure difference between engine and propellant tank govern the flow rate through the LAD and the amount of subcooling; both can affect the vaporization that may occur at the LAD screen and thus the localized temperature at the LAD screen.

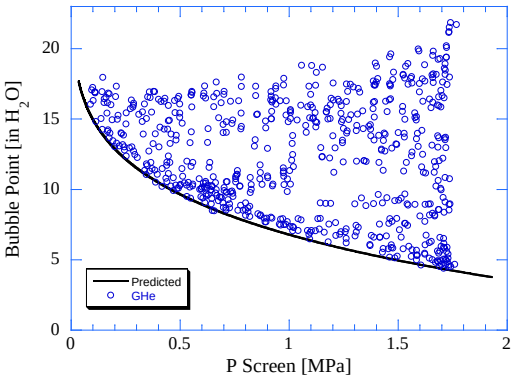

Figure 7: Pressure Dependence of Bubble Point for the 325x2300 Screen

To investigate the pressure dependence on bubble point, Figure 7 plots the data as a function of the liquid pressure at the screen. The theoretical value was determined using the surface tension based on the saturation temperature based on the pressure at the screen. As shown there is no direct pressure dependence using helium, since elevated bubble points in excess of 17 in H_2O are achievable for all pressures.

To further investigate this effect, Figure 8 replots the bubble point data from Figure 6 as a function of SD1 as a function of the pressure difference between screen and saturation pressure based on SD1. There are two distinct trends. First, bubble point data collected in near saturated liquid states all lie along the prediction curve from Equation (1) as indicated by the blue shaded region. Second, as the liquid becomes more subcooled, as this pressure difference increases, the experimental bubble points deviate from the normal prediction curve as indicated by the red shaded region. The highest bubble points of 20 in H_2O were obtained in the coldest liquid temperatures when the liquid was in its highest subcooled state consistent with facility limitations. Therefore Equation (1) holds for saturated liquid states and deviates proportional to the level of subcooling.

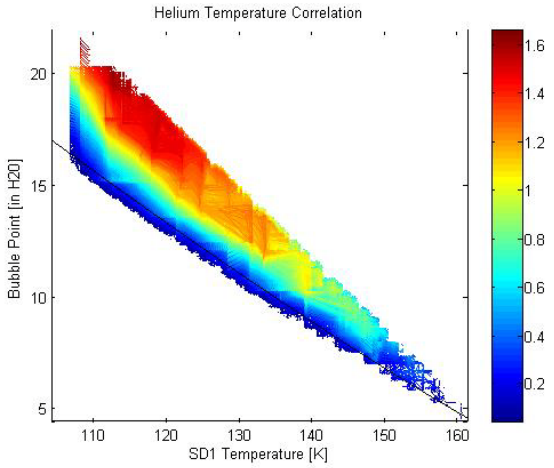

Figure 8: Temperature Correlation for Gaseous Helium at Bubble Breakthrough for a 325x2300 Screen. Color lines represent lines of constant $P_{SCREEN} - P_{SAT}(SD1)$ in units of [MPa].

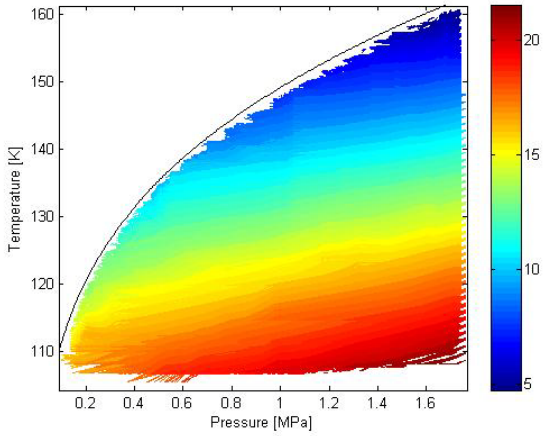

Figure 9: Combined Temperature and Pressure Dependence on Bubble Point Using Gaseous Helium as a Pressurant. Color represent regions of constant bubble point in units of [in H_2O].

To illuminate this subcooling effect, Figure 9 superimposes bubble point data on the plot of the thermodynamic test conditions (Figure 5) where the data is plotted as a function of liquid side screen pressure and temperature. Not only are larger values of bubble points obtained at colder temperatures, but also at higher pressures when comparing isotherms. Thus, the bubble point of LCH_4 for the screen can be increased by subcooling the liquid either by reducing its temperature or by increasing the pressure acting on the liquid.

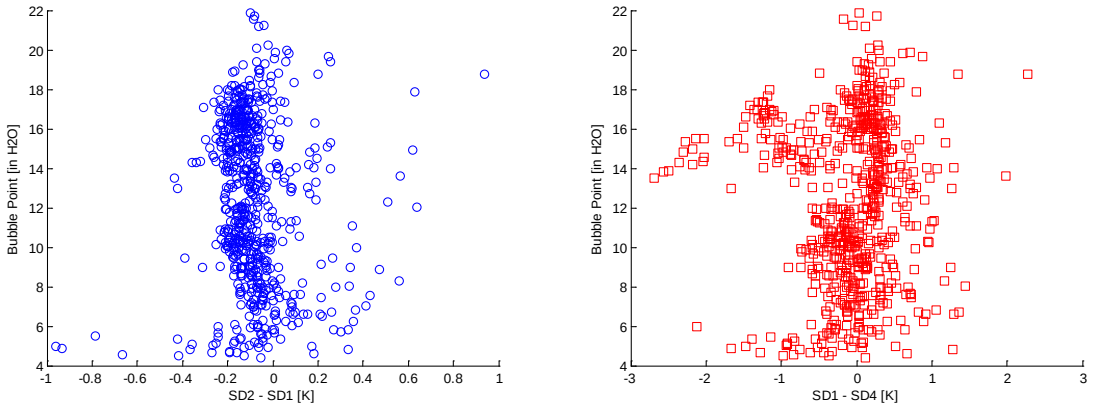

a b

Figure 10: Bubble Point Pressure as a Function of Temperature Differences (a) Across the Screen, SD2 – SD1, and (b) Within the Liquid Phase from the Screen to the Bulk Liquid Measurement Location, SD1 – SD4

To examine heat transfer at bubble breakthrough in the CFM test tank, Figures 10a and b plot the bubble point data as a function of the temperature differences across the screen (SD2 - SD1) and between the screen and bulk fluid (SD1 – SD4). For both figures, the temperature difference is nominally zero using GHe; but there are some interesting notes. For some of the test data, it is shown that the liquid side of the screen is slightly warmer than the gas side at bubble breakthrough. While the pressurant gas had enough residence time within the dewar and LAD screen/cup to decrease to LCH_4 temperatures prior to breakthrough, this negative temperature gradient across the screen was not anticipated. The temperature difference is still within the uncertainty of the diodes. Results from Figures 8 – 10 indicate that helium gas may be evaporating liquid away from the screen causing the liquid temperature to decrease at breakthrough, increasing the bubble point. Meanwhile the bulk liquid and screen liquid temperatures are nearly identical across the range of test conditions.

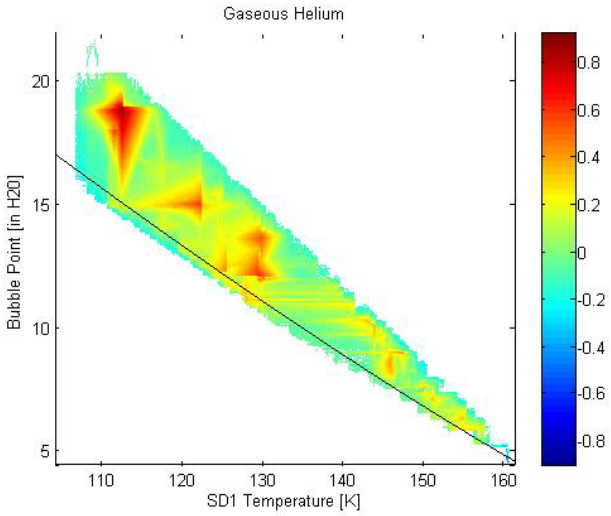

Figure 11: Bubble Point as a Function of the Liquid Screen Side Temperature and the Temperature Difference across the Screen. Color lines represent constant temperature gradients across the screen in units of [K].

Finally, Figure 11 plots the bubble point as a function of SD1 and as a function of the temperature gradient across the screen at breakthrough. As shown, there is relatively uniform heat transfer across the range of test conditions. Therefore bubble point is not a function of the temperature differences across the screen when the system is pressurized with GHe.

VIII. Plans

Future plans include analysis of LCH_4 bubble point data for the 325x2300 screen with gaseous nitrogen and methane as pressurant gases to compare with results obtained here using helium. In addition to the methane tests,

data was collected in LN_2 under an identical pressure range. Results for LN_2 will be compared to results in LOX and LCH_4 to construct a modified bubble point equation which faithfully predicts the trends outlined here.

IX. Conclusion

Bubble point predictions based on simple surface tension theory hold for saturated liquid states but fail to predict for subcooled liquid states. Across the full temperature range, bubble point is shown to be a strong function of liquid temperature that qualitatively scales with the surface tension of the liquid. However, the bubble point is higher than the predicted value when using GHe to pressurize the system. Pressurizing the LAD screen increases the bubble point proportional to the level of liquid subcooling. The discrepancy between model and data may be a result of helium evaporating liquid away from the screen at breakthrough, lowering the liquid temperature, and increasing the bubble point. There is shown to be a negligible temperature difference across the screen and into the bulk liquid over the range of conditions. This has implications in the design of LADs for in-space cryogenic propellant systems since pressurization with GHe yields a bigger margin in the total allowable pressure drop in a flight screen channel LAD system during fluid transfer from the propellant tank to the engine.

Acknowledgments

This work was funded by the Cryogenic Fluid Management Project at NASA Glenn Research Center under the auspices of the Exploration Systems Mission Directorate at NASA Headquarters. The authors would like to thank the operations team and research support staff at CCL-7 for their assistance during planning and testing phases.

References

[1] Fester, D.A., Villars, A.J., and Uney, P.E. "Surface Tension Propellant Acquisition System Technology for Space Shuttle Reaction Control Tanks" *AIAA-75-1196 11th AIAA/SAE Propulsion Conference*, Anaheim, CA, September 29 – October 1, 1975.

[2] Peterson, R. and Uney, P. "Development and Qualification of the Space Shuttle Orbiter Reaction Control System Propellant Tank" *AIAA-78-1026* AIAA/SAE 14th Joint Propulsion Conference, Las Vegas, NV, July 25 – 27 1978.

[3] Dickens, K. *Personal Correspondence with Kevin Dickens*, January 27, 2010.

[4] Marshall, W. and Kleinhenz, J. "Hot-Fire Testing of 100 lbf LOX/LCH4 Reaction Control Engine at Altitude Conditions" *5th JANNAF Liquid Propulsion Subcommittee Meeting*, May, 2010.

[5] Stiegemeier, B., Williams, G., Melcher, J.C., and Robinson, J. "Altitude Testing of an Ascent Stage LOX/Methane Main Engine" *5th JANNAF Liquid Propulsion Subcommittee Meeting*, May, 2010.

[6] Plachta, D., Jurns, J., Johnson, W., and Feller, J. "Methane Lunar Surface Thermal Control Test" *to be published.*

[7] Jurns, J.M., McQuillen, J.B., Gaby, J.D., and Sinacore S.A. "Bubble Point Measurements with Liquid Methane of a Screen Channel Capillary Liquid Acquisition Device" 54th JANNAF Conference, Denver, CO, May 14 – 17, 2007.

[8] Jurns, J.M. and McQuillen, J.B. "Liquid Acquisition Device Testing with Sub-cooled Liquid Oxygen" *AIAA-2008-4943* 44th Joint Propulsion Conference and Exhibit, Hartford, CT, July 21 – 23, 2008.

[9] Van Dyke, M. "Identification of Influential Factors for Liquid Acquisition Device Designs" *AIAA-98-3198*, 1998.

[10] Paynter, H. L. "Acquisition/Expulsion System for Earth Orbital Propulsion System, Vol. III, Cryogenic Test," Martin Marietta Corp., Denver, Colo., *MCR-73-97* 1973.

[11] Burge, G.W. and Blackmon, J.B. "Study and Design of Cryogenic Propellant Acquisition Systems – Volume II – Supporting Experimental Program" *NAS8-27685 MDAC Report MDC G5038* 1973.

[12] Cady, E.C. "Study of Thermodynamic Vent and Screen Baffle Integration for Orbital Storage and Transfer of Liquid Hydrogen – Final Report*"* *NASA-CR-134482* 1973.

[13] Cady, E.C. "Design and Evaluation of Thermodynamic Vent/Screen Baffle Cryogenic Storage System," *NASA-CR-134810* 1975.

[14] Cady, E.C. "Effect of Transient Liquid Flow on Retention Characteristics of Screen Acquisition Systems," *NASA-CR-135218* 1977.

[15] Chato, D.J. and Kudlac, M.T. "Screen Channel Liquid Acquisition Devices for Cryogenic Propellants," *AIAA-75-1196*, 38th Joint Propulsion Conference and Exhibit Indianapolis, IN, July 7-10, 2002.

[16] Kudlac, M.T. and Jurns, J.M. "Screen Channel Liquid Acquisition Devices for Liquid Oxygen," *AIAA-2006-5054*, 42nd Joint Propulsion Conference, Sacramento, CA, July 9 – 12, 2005.

[17] Hartwig, J.W. and McQuillen, J. "Analysis of Screen Channel LAD Bubble Point Tests in Liquid Oxygen at Elevated Temperature" *41nd AIAA Thermophysics Conference*, Honolulu, HI, June 27 – 30, 2011.

[18] Bretherton, F.P. "The Motion of Long Bubbles in Tubes" *Journal of Fluid Mechanics* 10, 166 – 188, 1961.

[19] Ferguson, A. and Kennedy, S. J., *Trans. Faraday Soc*., 32, 1936.